Optics Communications 284 (2011) 640–645

Contents lists available at ScienceDirect

Optics Communications

journal homepage: www.elsevier.com/locate/optcom

Ultrafast thermalization characteristics in Au film irradiated by temporally shaped femtosecond laser pulses

Guangqing Du, Feng Chen *, Qing Yang, Jinhai Si, Xun Hou

Key Laboratory for Physical Electronics and Devices of the Ministry of Education and Key Laboratory of Photonics Technology for Information, Shaanxi Province, School of Electronics and Information Engineering, Xi'an Jiaotong University, No. 28, Xianning West Road, Xi'an 710049, PR China

ARTICLE INFO

Article history:
Received 1 July 2010
Received in revised form 16 September 2010
Accepted 22 September 2010

Keywords:
Thermalization characteristics
Femtosecond pulse train
Two temperature relaxation
Thermal diffusion relaxation

ABSTRACT

The ultrafast thermalization processes of Au film irradiated by multi-pulse sequences with variable temporal separation were investigated by numerical simulations. Two temporally sequential thermal relaxation mechanisms including the two temperature relaxation and the thermal diffusion relaxation were demonstrated. With inclusion of the electron ballistic effect, we obtained the full 2-D temperature fields evolution dominated by the two distinct relaxation mechanisms. It is proposed that the laser thermalization processes can be greatly promoted through choosing the optimized temporal separation of the pulse train. We also found that the two temperature relaxation period can be modulated by changing the pulse train parameters such as the temporal separation, the pulse durations and the pulse number in a train.

1. Introduction

In recent years, femtosecond laser has become one of the most promising technologies in material processing because of the little collateral damage and heat conduction produced in the material [1–3]. For metal targets, it is believed that the potential advantages are physically originated from the distinct thermalization mechanisms for femtosecond pulses and nanosecond pulses ablation. In fact, the electron and phonon were out of equilibrium severely during the femtosecond laser pulses ablation, which potentially leads to the localization of laser energy deposition and the desired ablation precision. Because of the potential energy deposition merit, the femtosecond laser compared to nanosecond laser can well serve as the tool for accurately manufacturing of super high precision functional devices such as biochips, microfluidic channels and integrated optical circuit. However, unfortunately, many experimental investigations still demonstrated that the inaccuracy ablation due to melt and recast using a femtosecond laser can never be avoided completely [4–6]. In fact, the pulse separation of the commercial femtosecond amplifier is usually comparable to the melt and recast period of the target material, which potentially leads to the inaccuracy ablation. So, looking for a method to reduce the pulse separation for facilitating the excellent application of femtosecond laser becomes very urgently.

With recent advancement of laser pulse shaping techniques, especially those based on the nonlinear optical devices and the Fourier synthesis methods, almost arbitrarily shaped laser pulses in the amplitude and the phase can be produced [7,8]. Many potential applications emerged due to progress made in the pulse shaping techniques, such as the optimal control of chemical reaction [9], the enhanced ionization process [10] and the mass spectrometry analysis [11]. More recently, it is found that temporally shaped pulses train excitation enables new opportunities for optimal processing of materials [12]. A more precise manufacturing process can be achieved with such pulse train irradiation as observed by many groups in different materials [13–15]. For femtosecond laser ablation of metals, the diverse temperature relaxation mechanisms including the two temperature relaxation and thermal diffusion relaxation can be found to be responsible for the target thermalization in different timescales [16], whereas, it is believed that the two temperature relaxation, also called electron–phonon coupling relaxation mechanism plays an important role in the target thermalization process in high fluence regime [17]. So, understanding of the two temperature relaxation characteristics in the metal film is of great significance for the optimal material processing of metal targets. In fact, a large number of studies have been reported regarding the two temperature relaxation and its effects on laser–metal interactions [18–20]. However, with the temporally shaped pulses train excitation, namely multi-pulse sequences with variable separation, the ultrafast temperature relaxation characteristics, especially the two temperature relaxation properties are not exactly known and so far less investigated.

In this paper, we numerically investigated the ultrafast thermalization processes in Au film exposed to multi-pulses sequences. With temperature dependent thermal properties of Au film, the full 2-D temperature fields evolution in picosecond and nanosecond time domains were obtained, in which the target was irradiated by the

* Corresponding author. Tel./fax: +86 29 82665105.
E-mail address: chenfeng@mail.xjtu.edu.cn (F. Chen).

0030-4018/$ – see front matter © 2010 Elsevier B.V. All rights reserved.
doi:10.1016/j.optcom.2010.09.061

double pulse train with modulated temporal separation. The effect of the temporal separation of the pulse train on the non-equilibrium electron and phonon thermalization characteristics of the Au film was examined. Moreover, the dependence of the two temperature relaxation time on the pulse train parameters such as temporal separation, pulse durations and the pulse number was carefully analyzed. The results provide the theoretical guideline for enhancing the optimal laser energy deposition into the phonons of the Au target.

2. Modeling and method

2.1. Two temperature models

The well-known two temperature models which had been widely applied in investigation of ultrashort pulses interaction with metals are as follows [21]:

$$C_e\frac{\partial T_e}{\partial t} = \nabla(K_e\nabla T_e) - G\left(T_e - T_p\right) + Q \tag{1}$$

$$C_p\frac{\partial T_p}{\partial t} = G\left(T_e - T_p\right). \tag{2}$$

In Eq. (1), the temperature dependent electron heat conductivity is expressed as follows [22]:

$$K_e = \chi\frac{\left(\theta_e^2 + 0.16\right)^{5/4}\left(\theta_e^2 + 0.44\right)\theta_e}{\left(\theta_e^2 + 0.092\right)^{1/2}\left(\theta_e^2 + \eta\theta_p\right)} \tag{3}$$

here $\theta_e = T_e/T_F$ and $\theta_p = T_p/T_F$ are the normalized electron and phonon temperatures with T_F denoting the Fermi temperature; χ and η are material constants. For the high electron temperature, namely $\theta_e >> 1$, Eq. (3) results in the dependence $K_e \sim T_e^{5/2}$, which characterizes the low-density electron plasma. However, under the low temperature limit $\theta_e << 1$, the electron heat conductivity reduces to $K_e = K_0 T_e/T_F$ with K_0 means the electron thermal conductivity in room temperature. The heat capacity of electrons is assumed to be proportional to the electron temperature for the case of $T_e < 0.1T_F$ as can be found in the most existing works [23], i.e. $C_e = AT_e$. In Eq. (2), C_P is the phonon thermal capacity, considered as a constant here, and G is the electron–phonon coupling strength. The phonon heat conduction is normally ignored in the two temperature model due to the quite longer phonon diffusion period compared to the electron–phonon relaxation time.

The 2-D laser energy absorption rate Q is

$$Q = S(x,y)\cdot T(t) \tag{4}$$

where S and T represent the spatial and temporal energy absorption rates, respectively.

For a Gaussian spatial distribution laser beam, $S(x,y)$ is written as:

$$S(x,y) = \sqrt{\frac{4\ln 2}{\pi}}\frac{1-R}{t_p(\delta+\delta_b)}\frac{F}{n}\times\exp\left[-\frac{x}{\delta+\delta_b} - \left(\frac{y-y_0}{y_s}\right)^2\right] \tag{5}$$

here, R and δ are the wavelength dependent surface reflectivity and the optical penetration depth, $\delta_b = 100$ nm is the electron ballistic transport length for Au film. t_p is the FWHM (full width at half maximum) pulse duration, F is the total fluence of the pulse train. y_0 is the coordinate of the light front center at the target surface and y_s is the profile parameter.

The proposed model for prediction of the pulse train thermalization in Au film was also related in our previous works [16]. The main difference exists in the thermal source term in Eq. (1). Here, we only considered the temporal modulation of the pulse train, and the spatial shape of the pulse train is fixed as a Gaussian type. For the multi-pulse sequences, the temporal energy absorption rate can be described as

$$T(t) = \sum_{i=1}^{n}\exp\left(-4\ln 2\left(\frac{t-2t_p-(i-1)\Delta}{t_p}\right)^2\right) \tag{6}$$

where n is the pulse number in a train and Δ denotes the temporal separation between pulses in a train.

2.2. Normal thermal diffusion model

After the electron–phonon relaxation termination, the bulk temperature field evolution of the metal target is mainly dominated by the normal thermal diffusion mechanism which is represented by the following Fourier thermal diffusion equation:

$$C\frac{\partial T}{\partial t} = \nabla(k\nabla T) - \varepsilon\sigma\left(T^4 - T_0^4\right)d^{-1} \tag{7}$$

where C is the heat capacity of Au film in the electron–phonon equilibrium state, k is the heat conduction

$$k = 320.973 - 0.0111\times T - 2.747\times 10^{-5}\times T^2 - 4.048\times 10^{-9}\times T^3 \tag{8}$$

here, ε is the emissivity taken as 0.03 [24], σ is the Stefan–Boltzmann constant, d is the film thickness and T_0 is the ambient air temperature taken as 300 K in room temperature. The last term represents the radiation heat loss to the ambient environment, which could also be considered as the boundary condition. In fact, the heat loss to ambient environment is smaller in our calculation due to the slight temperature difference between Au surface and the ambient air.

2.3. Initial and boundary conditions

Because of the flexibility of finite element method FEM in dealing with the heat transfer equations, the coupling partial differential Eqs. (1) and (2) are simultaneously solved by the FEM. The calculation starts at time $t = 0$. The initial conditions for both electrons and phonons are assumed to be room temperature. Thus

$$T_e(x,y,0) = T_p(x,y,0) = 300\ \mathrm{K} \tag{9}$$

During the femtosecond-to-picosecond time period, it is reasonable to assume that heat losses from the metal film to the surrounding as well as to the front surface are neglected, and the perfect thermal insulation between Au film with substrate is assumed at the rear surface. Therefore, the boundary conditions can be written as

$$\left.\frac{\partial T_e}{\partial n}\right|_\Omega = \left.\frac{\partial T_p}{\partial n}\right|_\Omega = 0 \tag{10}$$

here, Ω represents the four borderlines of the 2-D Au film.

For the thermal diffusion model that works in the nanosecond timescale, the four boundaries of the 2-D Au film should be carefully considered for solving the normal thermal diffusion equation. We treat the radiation heat loss to the front surface as a built-in heat loss term during the thermal diffusion period as referred in Eq.(7), however, mathematically, we deal with thermal diffusion equation as thermal insulation at the front surface of the Au target. For the surrounding sides of the 2-D Au film, considering that the laser spot size is smaller compared to surface dimension of the target, the heat transfer dominated by the thermal diffusion mechanism can seldom reach the edges of the target, so it is reasonable to assume the thermal insulation at both surrounding sides in the nanosecond timescale; In addition, for the rear surface of the 2-D target, although a small quantity of heat energy can actually arrive at the rear surface of the Au

film during the nanosecond timescale, it is almost impossible for the weak heat wave to pass through the rear interface getting into the substrate because of large thermal resistance between the rear surface of the Au film and the substrate. Therefore, it is also appropriate to apply the thermal insulation condition at the interface between the Au film and substrate.

3. Results and discussion

The film thickness and width are taken as 3 μm and 8 μm, respectively. The material property parameters for the Au film are listed as follows [25]: $K_0 = 315$ W/(m K), $A = 2.1 \times 10^4$ J/(m^3 K), $C_p = 2.5 \times 10^6$ J/(m^3 K), $G = 2.6 \times 10^{16}$ W/(m^3 K), The laser related parameters we used are: $y_s = 1.5$ μm, $y_0 = 4$ μm, $\lambda = 800$ nm, $\delta = 15.3$ nm.

The non-equilibrium electron and phonon temperature fields evolution for the Au film triggered by double pulse train with temporal separation of 4 ps is shown in Fig. 1. We can see that the electron and phonon sub-systems are out of equilibrium dramatically at 200 fs, and the maximal electron temperature on the irradiated surface reaches 7000 K. However, the phonon sub-system of the Au film keeps undisturbed at this time, whose temperature is still close to the room temperature of 300 K. At time of 2 ps, the phonon temperature of the Au film begins to rise, and the electron temperature undertakes a severe drop. The maximal electron and phonon temperatures on the front surface of the Au film are 4174 K and 399 K, respectively. At time of 4.2 ps, the second pulse of the double pulse train strikes the Au film surface. It can obviously be seen that the electron temperature field takes on an abrupt enhancement, and climbs to the maximum value of 7805 K at the irradiated surface. It is indicated that the electrons sub-system gets out of the pre-existing non-equilibrium state again, and is stimulated to an even higher non-equilibrium state. However, the temperature field of the phonon sub-system keeps a regular ascending tendency, and the maximal phonon temperature at the front surface of the Au film gets 475 K at this time. It should be emphasized that the phonon temperature field penetrates into the deeper inner region at 4.2 ps, which means that the electron–phonon energy exchange dominates the temperature field evolution during this period. At time of 10 ps, the overheated electrons continuously dissipates it's energy to phonon due to the sustaining energy exchange between electron and phonon sub-systems dominated by the two temperature relaxation mechanism. The maximal electron and phonon temperatures on the irradiated Au film surface get 2949 K and 716 K, respectively. At time of 20 ps, the electron and phonon sub-systems get the thermal equilibrium state, and the maximal equilibrium temperature on the front surface of the Au film arrives at 794 K. It should be noticed that the phonon heat conduction and the radiation thermal loss to the ambient air had be rationally ignored because the two temperature relaxation time is quite shorter than the phonon thermal diffusion and the thermal radiation cycle. In fact, the phonon thermal diffusion and the thermal radiation mechanisms will play a more important role in the equilibrium thermal diffusion process of the Au film after the two temperature relaxation termination.

Fig. 2 shows the equilibrium temperature field evolution of the Au film following the two temperature relaxation termination. We can see that the temperature field significantly penetrates into the deeper

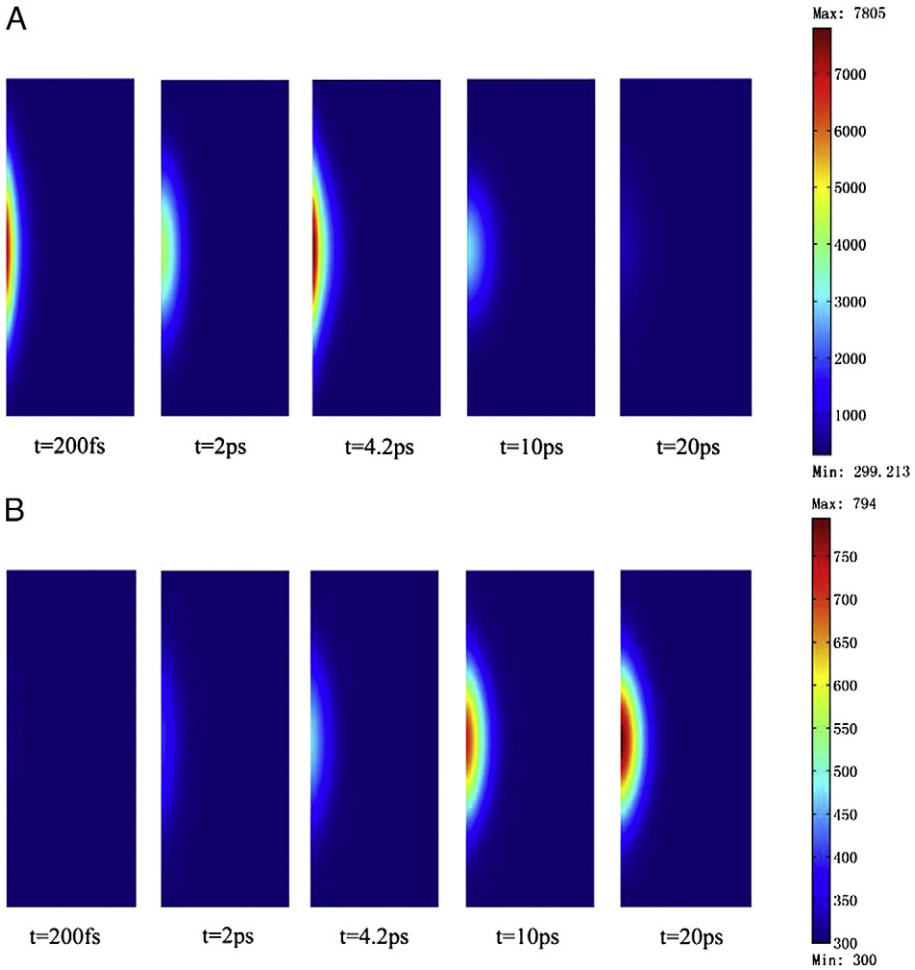

Fig. 1. Ultrafast 2-D non-equilibrium temperature fields evolution in Au film exposed to double pulse train. $R = 0.93$, $t_{p1} = t_{p2} = 100$ fs, $F = 0.8$ J/cm^2, $\Delta = 4$ ps. (A) Electron temperature fields. (B) Phonon temperature fields.

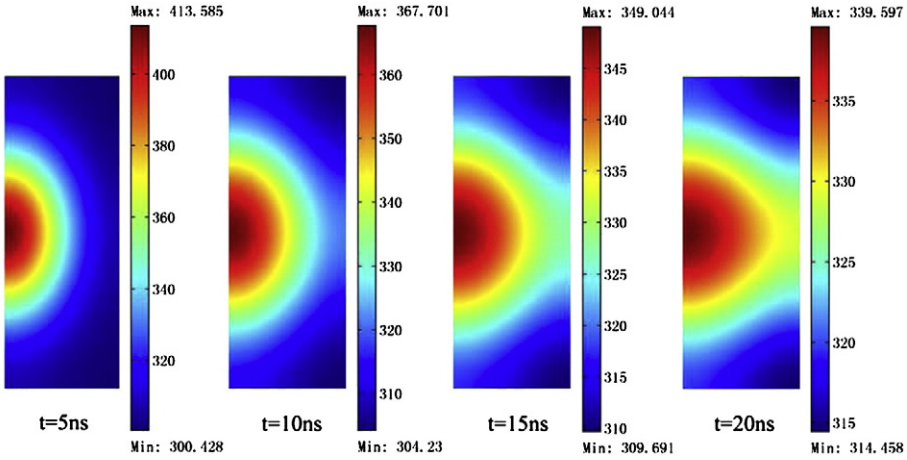

Fig. 2. Ultrafast 2-D equilibrium temperature fields evolution at different time after termination of two temperature relaxation.

inner region of the target at 5 ns, and the maximal temperature on the front surface of Au film sharply drops to 413.5 K. At time of 10 ns, the temperature field front arrives at the bottom of the Au film, and the maximal Au film temperatures on the front and rear surfaces come to 367.7 K and 322 K, respectively. At time of 15 ns, the Au film continues to dissipate its energy into the inner bulk. However, the diffusion speed of the thermal wave front slows down at this time, the maximal front surface temperature falls to 349 K and the rear surface temperature of the Au film slightly rises to 329 K. At time of 20 ns, the Au film temperature difference between the front and rear surfaces becomes marginal, indicating that the thermal diffusion relaxation mechanism driven by the temperature gradient is becoming more and more unimportant during this time. In this way, the Au film cools down, and ultimately gets thermal equilibrium with the ambient air.

The maximal surface electron temperature change vs. temporal separation of double pulse train for different fluences was shown in Fig. 3. We can see that the maximal electron temperature change decreases with increasing the temporal separation, and becomes constant once the pulse separation exceeds 10 ps. In our analysis, we assume that the change in reflectivity be proportional to the change in the electron temperature, $\Delta R \propto \Delta T_e$. This is particularly right for the case of the peak electron temperature change $\Delta T_{e\,\max} = T_{e\,\max} - T_0$, as proved experimentally [26]. So, we conclude that the laser energy deposition into the Au film can be promoted with increasing the temporal separation of the pulse sequences until it reaches to 10 ps as a result of the surface reflectivity reduction. It can be seen from Fig. 4 that when the separation of the double pulse train was less than 10 ps, the maximal surface phonon temperature increases intensely with increasing the separation, and once the temporal separation exceeds 10 ps, the phonon temperature performs a slow decrease. It should be emphasized that the optimal choice of almost the identical temporal separation will be both beneficial for laser energy absorption and subsequent phonon excitation processes, which potentially results in the enhancement of the laser thermalization process in the Au film target.

In fact, incubation effect of double pulses plays an important role in the enhancement of laser thermalization. As the pulse separation increases, the temperature profiles of the two successive pulses begin to overlap, and the incubation effect of previous pulse become significant. Once the pulse separation reaches the timescale comparable to the single pulse relaxation time of 10 ps, electron temperature responses to each laser pulses of the pulse train become independent, and the incubation effect of previous pulse vanishes. When the pulse separation continues to increase, the two temperature relaxation time rises and more thermal energy is transferred into the inner region of the target, so, as we see from Fig. 4, when the pulse separation exceeds 10 ps, the maximal surface phonon temperature decreases slowly with increasing the pulse separation.

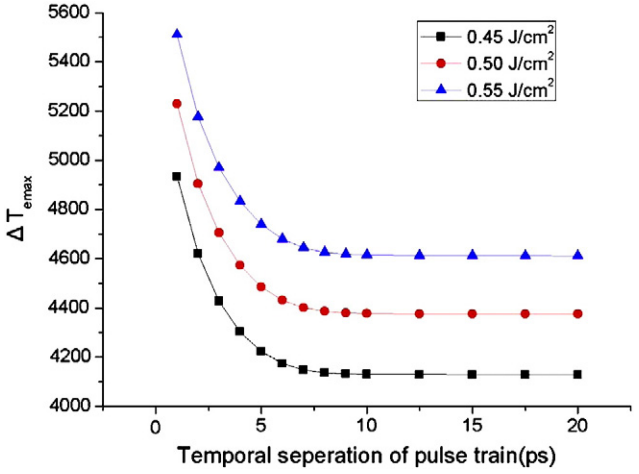

Fig. 3. Maximal Au film surface electron temperature change as a function of temporal separation of double pulse train for different laser fluences, $R = 0.93$, $t_{p1} = t_{p2} = 100$ fs.

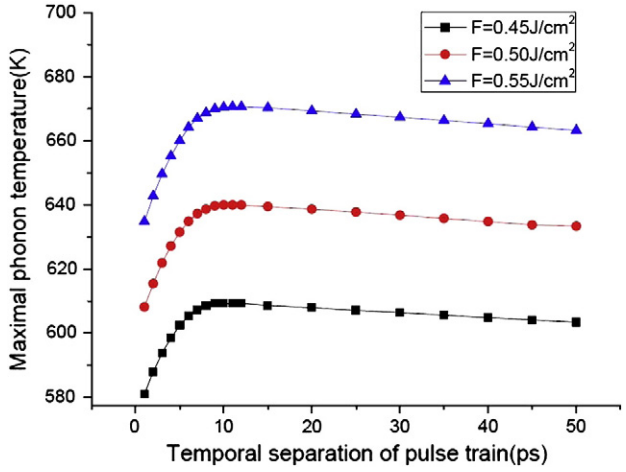

Fig. 4. Maximal Au film phonon temperature as a function of temporal separation of double pulse train for different laser fluences, $R = 0.93$, $t_{p1} = t_{p2} = 100$ fs.

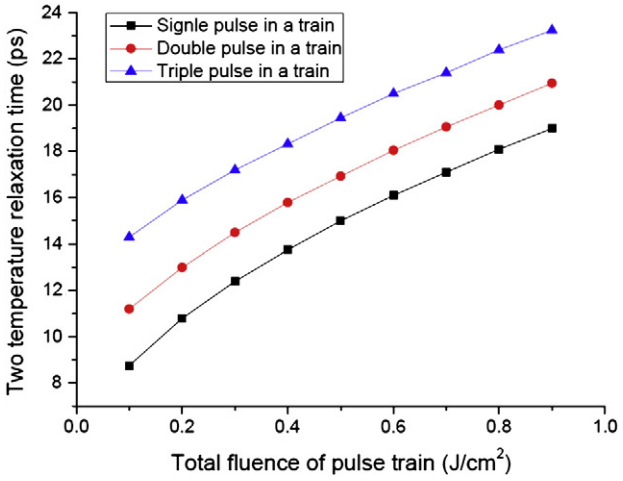

Fig. 5. Two temperature relaxation time as a function of total laser fluence of pulse train with different pulse number, $R=0.93$, $t_{p1}=t_{p2}=100$ fs, $\Delta=4$ ps.

Fig. 5 shows the two temperature relaxation time as a function of total laser fluence for three different pulse trains (including the single, double and triple pulse in a train). It is clearly suggested that the increase of total laser fluence can wholly lead to the significant increase of the two temperature relaxation time for the three different pulse trains, and a large pulse number in the pulse train also potentially causes the increase of the two temperature relaxation time. Fig. 6 shows the two temperature relaxation time as a function of the temporal separation of double pulse train for three different fluences. We can see that the two temperature relaxation time increases obviously with increasing the temporal separation of the pulse train for all laser fluences. The dependence of the two temperature relaxation time on the pulse duration for different pulse trains was shown in Fig. 7. We can see from Fig. 7(a) that the two temperature relaxation time increases slightly with increase of pulse duration in femtosecond time domain for the single, double and triple pulses in a train. However, it is different that the two temperature relaxation time increases violently with increasing the pulse duration in picosecond time domain for the three different pulse trains as shown in Fig. 7(b). Considering the fact that the heat deposition in the ultrashort pulses ablation process is mainly limited by the two temperature relaxation mechanism, so, the less dependence of the two temperature relaxation time on the pulse duration in femtosecond domain is greatly beneficial for the stable heat deposition into the Au film target, even though the pulse duration of pulse train is subjected to perturbation due to the material dispersion.

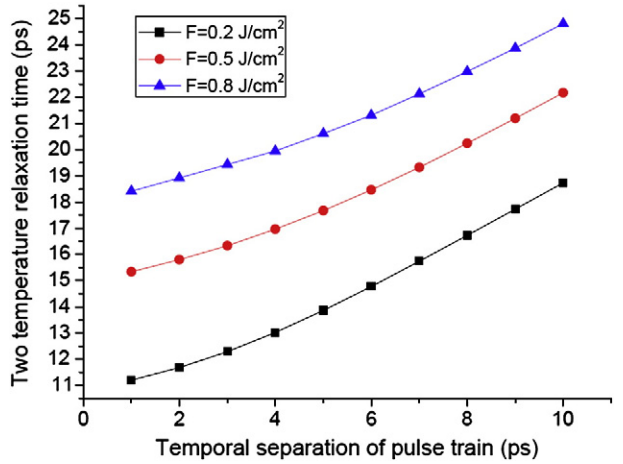

Fig. 6. Two temperature relaxation time as a function of the temporal separation of double pulse train for three different fluences, $R=0.93$ $t_{p1}=t_{p2}=100$ fs.

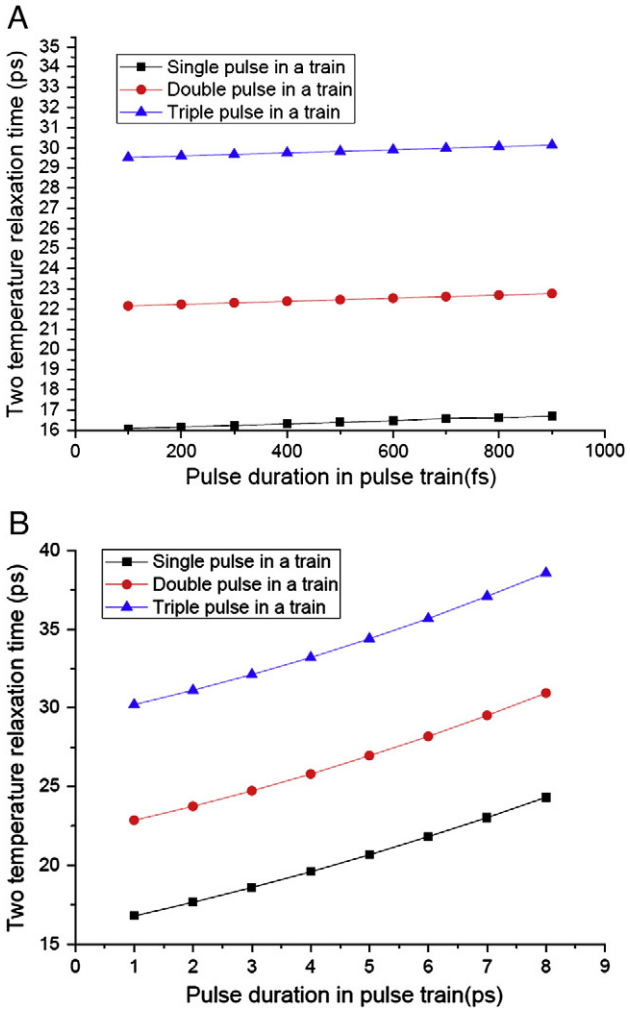

Fig. 7. Two temperature relaxation time as a function of pulse duration in a train with different pulse number, $R=0.93$, $F=0.6$ J/cm^2, $\Delta=9$ ps. (A) In femtosecond time domain. (B) In picosecond time domain.

4. Conclusion

In this paper, we numerically investigated the transient thermalization processes of Au film exposed to multi-pulse sequences with variable separation. The full 2-D temperature fields evolution processes including the two temperature relaxation and thermal diffusion relaxation evolution were obtained. It was revealed that the surface maximal electron temperature change during the two temperature relaxation period can be greatly reduced through increasing the temporal separation of the pulse train, which potentially results in the significant promotion of the laser energy deposition into the Au target. We also found that the maximal phonon temperature of the Au film can be significantly enhanced with the optimal choice of the pulse train separation. Moreover, it was shown that the two temperature relaxation time increases obviously with increasing temporal separation or total laser fluence of the pulse train, and a large pulse number also leads to the increase of two temperature relaxation time.

Acknowledgements

The work was supported by the National High Technology R&D Program of China under Grant No. 2009AA04Z305 and the National Science Foundation of China under Grant No. 60678011.

References

[1] R. Le Harzic, H. Schuck, D. Sauer, T. Auhut, L. Riemann, K. König, Opt. Express 13 (2005) 6651.
[2] N.N. Nedialkov, S.E. Imamova, P.A. Atanasov, G. Heusel, D. Breitling, A. Ruf, H. Hügel, F. Dausinger, P. Berger, Thin Solid Films 453 (2004) 496.
[3] X. Zhu, A.Yu. Naumov, D.M. Villeneuve, P.B. Corkum, Appl. Phys. A 69 (1999) S367 [Suppl.].
[4] A. Luft, U. Franz, A. Emsermann, J. Kaspar, Appl. Phys. A 63 (1996) 93.
[5] R. Le Harzic, D. Breitling, M. Weikert, S. Sommer, C. Föhl, F. Dausinger, S. Valette, C. Donnet, E. Audouard, Appl. Phys. A 80 (2005) 1589.
[6] F. Dausinger, RIKEN Rev. 50 (2003) 77.
[7] D.E. Leaird, A.M. Weiner, Opt. Lett. 29 (2004) 1551.
[8] A.M. Weiner, Rev. Sci. Instrum. 71 (2000) 1929.
[9] V.V. Lozovoy, Y. Andegeko, X. Zhu, M. Dantus, Chem. Phys. 350 (2008) 118.
[10] A. Castro, E. Räsänen, A. Rubio, E.K.U. Gross, Europhys. Lett. 87 (2009) 53001.
[11] T. Laarmann, I. Shchatsinin, P. Singh, N. Zhavoronkov, C.P. Schulz, I.V. Hertel, J. Phys. B Mol. Opt. Phys. 41 (2008) 074005.
[12] A. Semerok, C. Dutouquet, Thin Solid Films 453 (2004) 501.
[13] R.L. Harzic, D. Breitling, S. Sommer, C. Föhl, K. König, F. Dausinger, E. Audouard, Appl. Phys. A 81 (2005) 1121.
[14] T.Y. Choi, D.J. Hwang, C.P. Grigoropoulos, Appl. Surf. Sci. 197 (2002) 720.
[15] I.H. Chowdhury, X. Xu, A.M. Weiner, Appl. Phys. Lett. 86 (2005) 151110.
[16] G. Du, F. Chen, Q. Yang, J. Si, X. Hou, Opt. Commun. 283 (2010) 1869.
[17] J. Güdde, J. Hohlfeld, J.G. Müller, E. Matthias, Appl. Surf. Sci. 127 (1998) 40.
[18] W.S. Fann, R. Storz, H.W.K. Tom, J. Bokor, Phys. Rev. Lett. 68 (1992) 2834.
[19] S.-S. Wellershoff, J. Hohlfeld, J. Güdde, E. Matthias, Appl. Phys. A 69 (1999) S99 [Suppl.].
[20] R.H.M. Groeneveld, R. Sprik, A. Lagendijk, Phys. Rev. B 51 (1995) 11433.
[21] S.I. Anisimov, B.L. Kapeliovich, T.L. Perel'man, Sov. Phys. JETP 39 (1974) 375.
[22] J.K. Chen, W.P. Latham, J.E. Beraun, J. Laser Appl. 17 (2005) 63.
[23] I.H. Chowdhury, X. Xu, Numer. Heat Transf. A 44 (2003) 219.
[24] L. Jiang, H.L. Tsai, Int. J. Heat Mass Transfer 50 (2007) 3461.
[25] T. Liu, W. Dai, Int. J. Therm. Sci. 48 (2009) 34.
[26] H.E. Elsayed-Ali, T. Juhasz, Phys. Rev. B 47 (1993) 13599.